ACS APPLIED POLYMER MATERIALS

pubs.acs.org/acsapm

Article

Controlled Environment Neutron Radiography of Moisture Sorption/Desorption in Nanocellulose-Treated Cotton Painting Canvases

Alexandra Bridarolli,* Marianne Odlyha, Genoveva Burca, John C. Duncan, Freddie A. Akeroyd, Andie Church, and Laurent Bozec

Cite This: *ACS Appl. Polym. Mater.* 2021, 3, 777−788

Read Online

ACCESS | Metrics & More | Article Recommendations | Supporting Information

ABSTRACT: Nanocellulose-based materials have recently been used to consolidate degraded cotton painting canvases. Canvas-supported paintings consist of materials that are sensitive to moisture and especially susceptible to environmental fluctuations in temperature and relative humidity (RH). These environmental fluctuations occur in uncontrolled environments found in historic houses and palaces and can lead to hydrolytic degradation and mechanical damage to canvases. To simulate this situation in an experimental setting, canvas samples were mounted in a custom-made closed-cell and subjected to programmed cycles of RH at a controlled temperature while exposed to the neutron beam. Results are presented for both untreated samples and those treated with a polar consolidant, cellulose nanofibrils (CNF(aq)) in water, and an apolar consolidant, a composite of persilylated methyl cellulose with surface silylated cellulose nanocrystals (MC+CNC(h)) in heptane. They were then compared with changes in ionic conductivities as measured by dielectric analysis (DEA) with the same cyclic RH program and temperature. Although the samples were exposed to the same experimental conditions, they presented treatment-specific responses. CNF-treated canvas showed higher hygroscopicity than the untreated sample and facilitated moisture diffusion across the sample to areas not exposed to the environment. A sample treated with MC+CNC(h) retarded moisture diffusion during the increase in RH and could, therefore, afford protection to moisture absorption in uncontrolled environments. Thus, the experimental setup and resulting data provide a pilot study demonstrating the potential of neutron radiography in following and comparing real-time moisture diffusion dynamics in untreated and nanocellulose-consolidated cotton canvases and assisting in validating the overall benefit of the treatment.

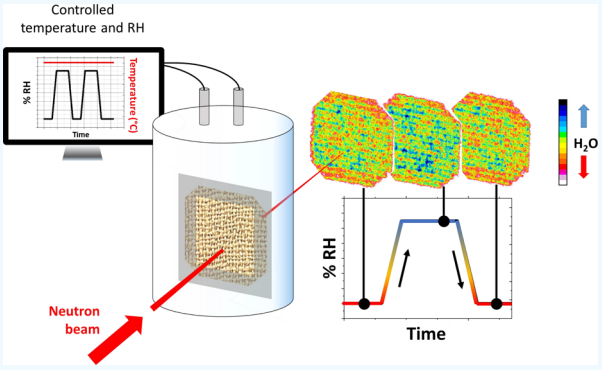

KEYWORDS: *neutron radiography, moisture sorption and desorption, cyclic RH, canvas, nanocellulose, consolidant, dielectric analysis*

INTRODUCTION

The long-term preservation of paintings relies on controlling their surrounding environmental conditions (on display and in storage) and on applying a specific conservation treatment tailored to the painting to be preserved. In both cases, moisture plays a role, and it is essential to understand how rapidly moisture can diffuse into a painting. When paintings are displayed in uncontrolled environmental conditions, as found in historic houses and palaces, fluctuations in relative humidity (RH) can lead to cracking of the paint layer and enhanced hydrolytic damage to the supporting canvases.[1] In the worst case, the RH fluctuations will result in a loss of paint accompanied by a loss in strength and elasticity of the painting canvases. Upon reaching this stage of damage, the canvas can no longer effectively support the paint structure.[2] Some conservation treatments for damaged paint layers have used a moisture-based approach. During this treatment, localized areas of the surfaces of paintings are in contact with enhanced water vapor levels.[3,4] For canvases, conservators have traditionally lined damaged canvases. This procedure was routinely performed until its associated risks were identified, especially those related to the invasiveness of the traditional consolidants.[5] In an attempt to provide an alternative to lining, conservators started introducing synthetic consolidants such as BEVA 371, a widely used poly(ethylene vinyl acetate)-based heat-seal adhesive[6] as part of their consolidation approach. Yet, the long-term merits of such synthetic consolidants are also

Received: September 24, 2020
Accepted: January 5, 2021
Published: January 29, 2021

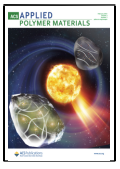

questioned due to the instability and irreversibility of some of these materials.[7,8] Thus, the field is still searching for novel consolidation strategies based on more eco-friendly materials to fulfill current practice requirements. Current interest now focused on novel nanocellulose-based materials.[9,10] Their use for conservation treatment has been recently explored in the framework of the EU Nanorestart project (http://www.nanorestart.eu/, accessed 25/08/20). In this project, which encompasses this study, nanocellulose has been proposed as a new approach to canvas consolidation.[11,12] Nanocellulose-based materials have attracted a lot of attention on account of their excellent mechanical properties,[13,14] high surface area, abundant hydroxyl groups, which can be readily functionalized,[15] and their environment-friendly sourcing.[16] Nanocellulose is also chemically compatible with artists' canvases made of natural fibers such as cotton, linen, or jute, which are themselves cellulosic materials. As such, both the canvas and the nanocellulose treatments are responsive to moisture.

The work presented here follows an initial study that focused on the evaluation of the adhesion and performance of a naturally sourced nanocellulose consolidant, i.e., cellulose nanofibrils (CNF).[17] This study, as well as others that followed,[12,18] involved the use of dynamic mechanical analysis (DMA) with controlled RH to evaluate the effect of fluctuations in RH on the viscoelastic properties of degraded cotton canvases treated with a variety of nanocellulose consolidants. The programmed RH cycles were applied to simulate enhanced effects of environmental fluctuations as it has been shown that changes in humidity levels induce stresses in paintings, which can lead to the development of microcracks and flaking of paint.[19,20] This type of testing was applied for the first time on canvas and demonstrated how the treatments affected the physical and mechanical response of the treated canvases at high humidities (RH circa 80%) and with an increasing number of RH cycles.[18] However, these tests did not image the spatial distribution of moisture in these canvases. For this reason, neutron radiographs of the samples in a controlled environment were taken with a sample cell specially designed for this experiment using programmed changes in RH.

Neutron radiography is a non-destructive and non-invasive technique that generates two-dimensional (2D) images. The imaging technique is based on the attenuation (absorption and scattering) of a neutron beam as it passes through the sample. The relationship between the incident intensity I_0 and the transmitted intensity I is given by the Beer–Lambert law defined as

$$I = I_0 \, e^{-\mu t} \tag{1}$$

where μ is the attenuation coefficient along the path of the neutron through the sample (depends on the selected material and its density) and t is the thickness of the sample along this path.

Neutrons interact strongly with only a few chemical elements, the most prominent being hydrogen, which strongly attenuates them. The direct interaction between neutrons and hydrogen makes them ideally suited for imaging moisture transport. The study of this interaction has led to a variety of applications and includes soil and plant water distribution, which have been readily imaged.[21,22] Other work involved mapping the water uptake and vapor diffusion through wood adhesives.[23] In conservation research studies, neutrons have been used to study water uptake in painting canvases and preparation layers and to visualize the spatial distribution of moisture in paintings.[24] To date, the standard setup to study the diffusion behavior of water vapor in a material has relied on the dry cup/wet cup experimental setup. For example, the diffusion of moisture in the longitudinal axis of wood samples was investigated by sealing one side of the sample to a recipient containing silica gel ("dry cup") or saturated salts ("wet cup") while the other side of the sample was exposed to the environment of a closed chamber.[25] The climate in the chamber was regulated with two basins filled with demineralized water or saturated salt solutions (depending on the desired humidity). A similar setup using the dry and wet cups and a chamber at 23 °C and 50 ± 2%RH was later used by Hendrickx[26] to study mock-ups of an easel oil painting. The environmental conditions in this type of experiment were therefore fixed and could not be varied without having to stop the neutron beam, prematurely ending the experiment. This had the disadvantage of not enabling the measurement of dynamic stages of the diffusion process, namely, the moisture sorption and desorption steps.

The use of RH-controlled chambers was introduced to address this problem as described in Hendrickx et al.[27] In their study, they used a miniature climatic chamber, which allowed control of RH between 10% and 95% so that absorption and desorption could be imaged. A climatic chamber was also designed by Mannes,[28] which allows the programming and remote control of the RH and temperature conditions inside the chamber in both static (fixed relative humidity RH) and dynamic mode (cycles in RH). Being able to control the temperature is essential in diffusion studies as both water diffusion and moisture content are greatly influenced by temperature. This influence was demonstrated for plant fibers, in which the moisture content increases as a result of a decrease in temperature at constant RH level.[29,30]

Dielectric analysis was also used in this study to monitor the absorption and desorption of moisture. Doing so enabled us to perform a direct comparison and validation of the results obtained by neutron radiography. This technique is used for characterizing polymeric materials and is particularly useful as it has a high sensitivity for polar substances present. An AC electrical field is applied to the parallel plates, and the complex relative permittivity can be resolved into real and imaginary components. Measurements are typically made over a range of frequencies. The use of multiple frequencies permits the calculation of the ionic conductivity using

$$\sigma' = \omega \varepsilon_o \varepsilon'' \tag{2}$$

The real part of the complex conductivity, σ', is related to the imaginary part of the permittivity, ε'', i.e., the dielectric loss, as shown above. ε_o is the permittivity of free space, 8.85 pFm^{-1}, and ω is the angular frequency.

It is known that the properties of cellulose, in particular, its conductivity (σ') are highly dependent on moisture content. A recent study[31] describes how the electrical conductivity (σ') of cellulose increases with increasing water content. This is explained by the formation of a conductive water-cellulose pathway along which ions could move.

Our work aimed to monitor moisture uptake/loss and map its distribution during controlled and programmed cycles of moisture sorption and desorption in small canvas samples. A custom-made humidity-controlled chamber was designed for the neutron radiography experiments. Unlike the previous work, the sample cell used in our study took the shape of a

https://dx.doi.org/10.1021/acsapm.0c01073
ACS Appl. Polym. Mater. 2021, 3, 777−788

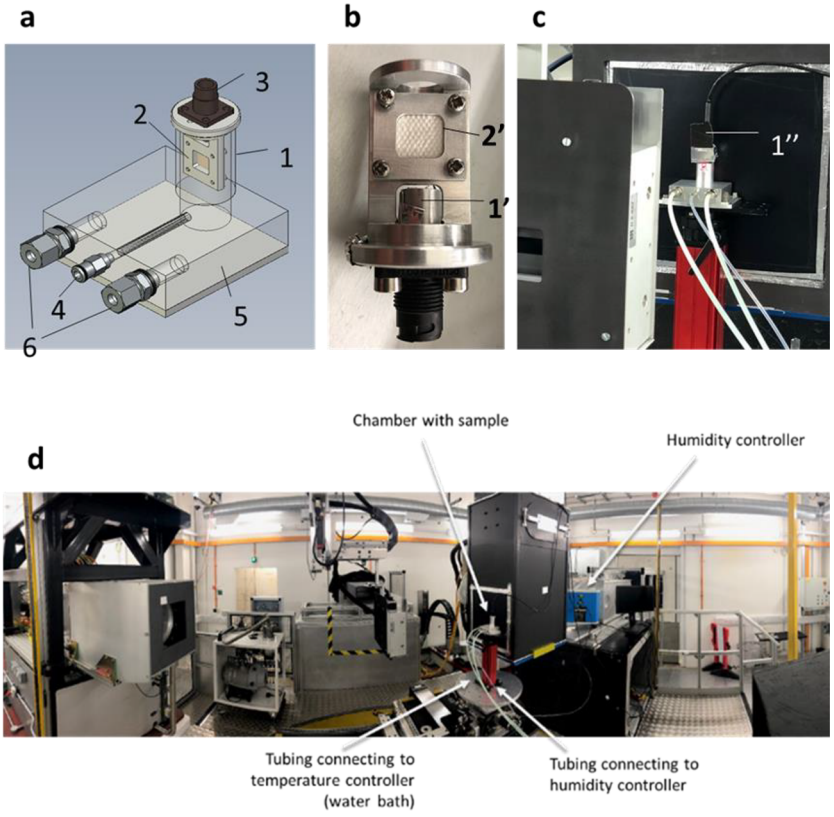

Figure 1. Cylindrical chamber with sample frame (a) (1 and 2) (grade 6082T2 aluminum). The frame was welded to the cylinder lid. The RH sensor previously calibrated was inserted at the top (3) and was connected via cable to the RH controller (tuned to dimensions of sample cell). The RH inlet was connected via tubing (flow 0.6 L/min) at the bottom (4). Compartment with controlled T (5). Leads inlet and outlet (6) connect to the water bath to control the temperature. The RH sensor protected from neutron beam marked 1′, 1″ (b and c). Shown in (d) is the panoramic view of the experimental setup. This shows the location of the chamber with sample and tubing connected to the temperature controller (water bath) and the humidity controller.

small cylinder into which the sample frame was lowered (Figure 1). The chamber was connected to a commercial RH controller (Lacerta Technology, UK), which provided a linear programmed ramping of the RH at a selected rate and to a recirculating water bath (providing temperature control). This was the first time that neutron radiography measurements under a controlled environment were performed on IMAT beamline at the ISIS Neutron and Muon Spallation Source, UK. The data collected were correlated with changes in ionic conductivities measured using dielectric data under the same RH cycling program.

This study supplements previous investigations[12,18] looking into the efficacy of novel nanocellulose-based consolidants for modern easel paintings used as a possible alternative to lining while protecting the canvases from environmental RH fluctuations. To date, the assessment of new materials used in conservation practice lacks a deeper understanding of their response to moisture sorption and desorption. It is anticipated that the neutron radiography experiments will provide information on the response to RH fluctuations and how the moisture is distributed within both the untreated and treated canvases. This study also establishes a proof of concept to validate the use of neutron radiography for dynamic measurements of sorption/desorption processes of moisture in painting canvases and to evaluate the effect of novel canvas treatments on these processes.

MATERIALS AND METHODS

Samples. Three series of samples were prepared as follows: modern degraded cotton canvas untreated (control sample), treated with a polar consolidation agent, cellulose nanofibrils (CNF) dispersed in water or treated with an apolar consolidation agent, persilylated methyl hydroxyethyl cellulose combined with surface silylated cellulose nanocrystals (MC+CNC(h)) in heptane.

Canvas. In this study, the commercial cotton canvas (Barna Art, Barcelona, Spain) used consisted of a plain-woven fabric of 341 ± 1 g/m^2 and presented 9 and 11 threads/cm in the warp and weft directions, respectively. The cotton sample was chemically degraded according to a protocol described elsewhere.[32] The degree of polymerization (DP) of the prepared aged canvas was ca. 500. This DP value is low compared to the DP of canvases made of different proportions in bast, ramie, and linen fibers, which were considered in "good conditions" and present a DP superior to 1000.[1]

Consolidation Treatments. These canvases were then subjected to a consolidation treatment, consisting of a prepared nanocellulose dispersion of CNF provided by Stora Enso AB (Sweden). The composite treatment consisting of persilylated methyl hydroxyethyl cellulose and surface silylated crystalline nanocellulose (MC+CNC-(h)) at 1.98%w/w, in heptane, was obtained from the Zentrum fur Bucherhaltung (ZfB, Leipzig, Germany). The procedure used for the silylation of the two compounds, and the introduction of hydrophobic groups, which enables their dispersion or dissolution in nonpolar solvents, is described elsewhere.[33] The crystalline nanocellulose, i.e., CNC (CelluForce NCC) was purchased from CelluForce Inc. The treatments were applied by brush on both sides of the canvas. Surface coverages of 30 and 15 g/m^2 (i.e., 8.8% and 4.4% weight increase in canvas weight) were reached after complete drying of the treatment. The calculation of the required amount of consolidant needed was

https://dx.doi.org/10.1021/acsapm.0c01073
ACS Appl. Polym. Mater. 2021, 3, 777−788

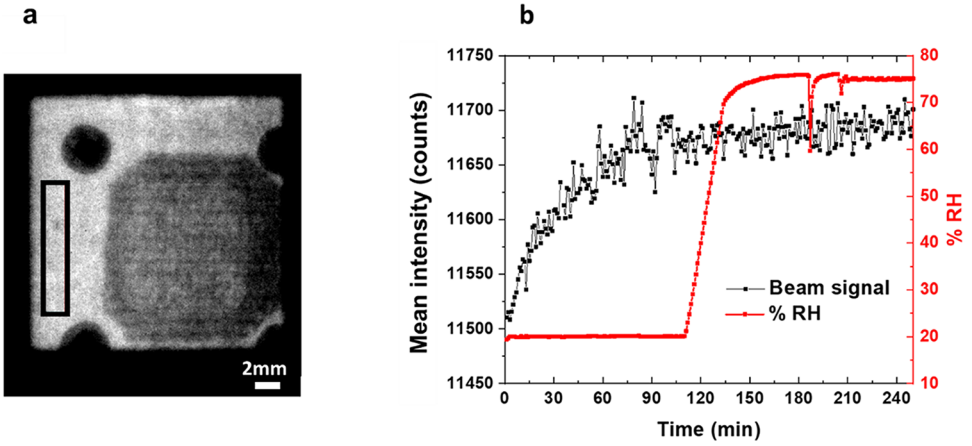

Figure 2. (a) Image of frame supporting the CNF-treated canvas. (b) Mean intensity of neutron beam signal measured over time is shown in for an area (black rectangle marked in (a)) on an area beside the canvas sample. The instability of the beam signal can be clearly seen in (b). This is problematic as it interferes with the true response of the sample to moisture variations.

performed for each product prior to their application. An increase in sample thickness from 0.848 mm to 0.880 mm (+4%) and to 0.906 mm (+7%) was measured using a digital micrometer for the cotton canvas before and after treatment with CNF and MC+CNC(h), respectively.

Neutron Radiography. *Sample Chamber.* The sample chamber used in these tests was designed by Lacerta Technology (UK) (Figure 1a). The frame containing the sample is presented in Figure 1b. As seen in Figure 1a, the cell consists of a cylindrical chamber (1) of 20 mm in diameter and 56 mm in length in which a frame holding the sample (ca. 13 × 13 mm^2) in place can be inserted (2). The sample is directly exposed to the chamber environment through the 10 × 10 mm^2 window (Figure 1b(2′)). Samples were all oriented the same way (i.e., weft = horizontal, warp = vertical). The upper tube containing the sample as well as the frame were both made from grade 6082T2 aluminum so that the cell would be transparent to the neutrons. The frame was welded to the cylinder lid so that the chamber could be tightly closed for the accurate control of the RH in the chamber during the experiment. The RH sensor, which was connected to the RH controller, was placed on top of the sample and chamber [(3) in Figure 1a and Figure 1b]. The RH inlet came via tubing (flow 0.6 L/min) from the bottom of the chamber (Figure 1a(4) and Figure 1c). The RH sensor was calibrated using a Michell Optical Humidity & Temperature Calibrator based on the chilled mirror principle (http://www.michell.com/uk/products/optiCal.htm, accessed 25/08/20). The signal from the RH sensor was used to control the RH controller directly to maintain a constant RH environment in the cell.

The temperature was controlled and maintained constant at 25 °C via water circulating inside the rectangular base of 75 × 75 × 24 mm^3 (Figure 1a(5)), which was in direct contact with the sample cylinder, ensuring a uniform temperature throughout. The humidity cell was connected to a recirculating water bath via two 6 mm diameter pipes (water inlet and outlet) (Figure 1a(6)) to a recirculating water bath. The RH controller was tuned to the specific requirements of the cell built for this experiment to give optimal control, with minimal lag and overshoot. Moreover, the RH sensor was protected from the neutron beam using cadmium foil (Figure 1b(1′)) and boron carbide (Figure 1b(1″)) as neutron shielding. Figure 1d shows the complete setup as used during the neutron experiments.

Experimental Setup. The measurements were carried out at the ISIS Neutron and Muon Spallation Source, UK at the neutron imaging beamline IMAT (Imaging and Materials Science & Engineering).[34,35] The neutron radiographies were collected with an optical camera box[36] based on a 2048 × 2048 pixels Andor's Zyla sCMOS 4.2 Plus camera. The chamber was positioned as close as possible to the ZnS/LiF scintillator to reduce penumbra blurring. An L/D of 250 was used, where L (10 m) is the distance between the pinhole selector and the chamber and D (40 mm) is the pinhole's diameter. The beam was shaped by using five pairs of jaws available on IMAT to the chamber size (50 × 50 mm^2) to avoid the electronics radiation. The exposure time was set to 30 s per image, and a spatial resolution of 53 μm was achieved.

The software IBEX Instrument Control software[37] from ISIS was modified in collaboration with Lacerta Technology to ensure that simultaneous RH readings were obtained with the corresponding beam images. This was a novel addition to the IBEX software, which permitted the correlation of RH readings with neutron image data a much more straightforward task, and removed possible errors in the synchronization of the data streams from two independent devices.

RH Program. Prior to mounting, the samples were pre-dried for at least 24 h. During the experiment, the samples were subjected to one or two RH cycles (20−75−20%), consisting of 30 min RH equilibration at 20%RH followed by an increase in RH at 4%RH/min to 75%RH. The RH remained at 75% for 90 min for the experiments before being reduced at 4%RH/min to 20%RH.

Image Processing. Image processing was automated using a macro written for ImageJ (version 1.53) specifically for the images obtained from these measurements and setup.[18]

Dielectric Analysis under Controlled RH (DEA-RH). Dielectric analysis with cyclic programmed RH was used to test the above samples, and the same RH program as for the neutron radiography experiment (20−75%RH, 25 °C) was employed. Three replicas were measured for each sample. The canvas samples (13 mm × 13 mm and ≈1 mm thick) pre-dried for at least 24 h using silica gel were measured at four different frequencies (0.3, 1, 3, and 10 kHz) by applying an alternating electrical field to the electrodes of a Lacerta Technology DS6000 Dielectric Analyser connected to the Lacerta Technology RH controller. The flat canvas samples were placed between the lower spring-loaded 33 mm diameter electrode and the upper fixed 10 mm diameter electrode. Adjusting the lower electrode position changes the spring pressure applied to the electrode and sample. This was set to the same position for all samples to ensure a consistent pressure was applied to all samples.

RESULTS AND DISCUSSION

Intensity Correction of the Neutron Images. Neutron radiography of the CNF-treated sample is shown in Figure 2a. An area on the frame supporting the CNF-treated canvas was selected (black rectangle), and the variations in beam signal measured over time in this area are shown in Figure 2b.

From Figure 2a, it is clear that the mean intensity (hence beam signal) measured in the indicated area is not stable with time. This signal was, therefore, used to account for beam signal instability and was included in the protocol used for

https://dx.doi.org/10.1021/acsapm.0c01073
ACS Appl. Polym. Mater. 2021, 3, 777−788

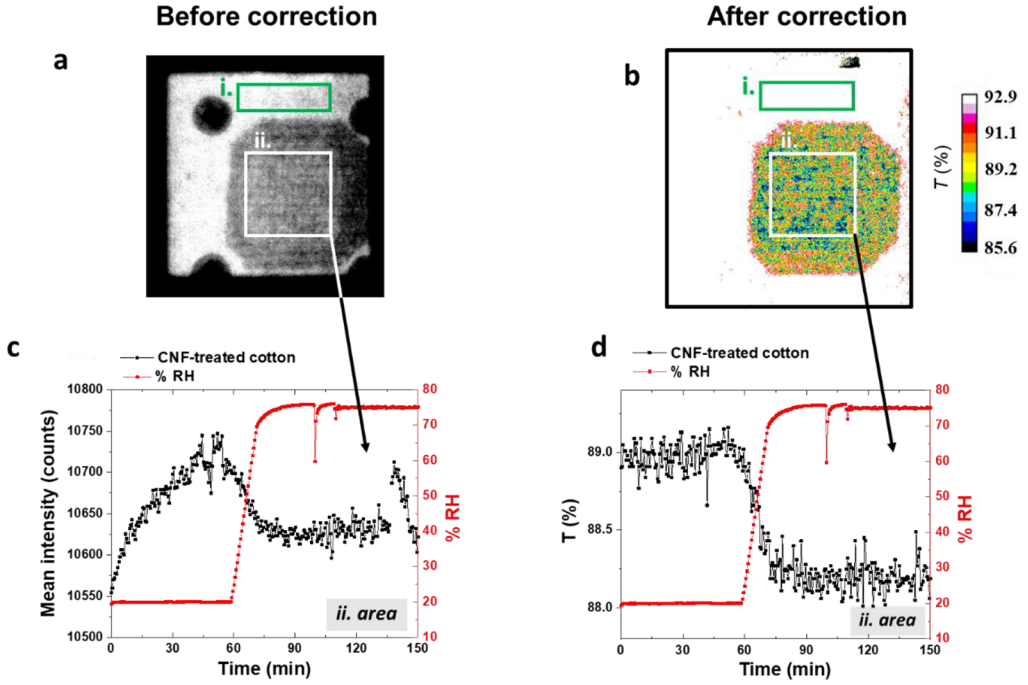

Figure 3. Neutron radiography image (a) together with mean intensity (c) or percentage transmission ($T(\%)$) (d) vs time of the CNF-treated sample exposed to a 20−75%RH step (4%RH/min) before (a and c) and after image correction (b and d). A selected area on the sample (white square indexed ii. in (a) and (b), 7.4 × 7.4 mm^2) corresponding to an area directly exposed to the chamber environment was used to integrate the mean intensity for the raw images. An area beside the sample (green rectangle indexed i.in (a)) was also measured to check the correction and verify that results were not altered by variations in moisture level in the chamber. Results are given in the Supporting Information (Figure S1a).

image correction. The neutron radiographies collected were converted to neutron transmission images by subtracting the sCMOS camera dark current offset and then dividing by the flatfield images accounting for spatial variation of the illuminating neutron beam and scintillation inhomogeneity. This operation consisted of the following correction steps:[38]

1. Correction accounting for beam signal instability and subtraction of dark image following eq 3:
   - Calculation of the mean value $D(I_n)$ of the intensity, or scaling factor, as measured inside the black rectangle, in an area beside the sample on the frame (Figure 2a) for neutron radiography in position n (I_n) [where 1 < n < "total number of images"].
   - Subtraction of the dark image (I_{dark}), i.e., image captured with the shutter closed, from the neutron radiography of the sample n (I_n).
   - Division by correction factor $D(I_n) - D(I_{dark})$, where $D(I_{dark})$ is the mean value of the intensity in the black rectangle with the shutter closed (Figure 2a) for mean of 60 dark images:

$$I_{corr,n} = \frac{(I_n - I_{dark})}{D(I_n) - D(I_{dark})} \quad (3)$$

where I_n is the raw data for sample's radiography, I_{dark} is the data for the image obtained with all shutters closed, $D(I_n)$ is the scaling factor (as above), and $D(I_{dark})$ is the scaling factor of the image captured with the shutter closed.

Neutron exposure normalization was performed by deriving a scaling factor $D(I_n)$ in an open beam region of interest, i.e., a small image area beside the object under investigation (black rectangle in Figure 2a). This correction scales the measured radiograph so that the same neutron source intensity is assumed for all radiographs of a series. The dark image that corresponds to a picture of the sample taken with the shutter closed was also subtracted to the neutron radiograph. This correction removes the signal, current, and noise generated by the camera and related electronics.

2. Noise removal was performed using the outlier removal plugin of ImageJ (radius = 2, threshold = 500). White and dark spots due to gamma radiation or pixel failures from the radiographs were successfully removed while preserving the features of the woven canvas.
3. Flat-field correction eliminates the beam variation and camera noise. This correction was done following eq 4:

$$I_{norm,n} = \frac{I_{corr,n}}{I_{corr,flat}} \quad (4)$$

using

$$I_{corr,flat} = \frac{(I_{flat} - I_{dark})}{D(I_{flat}) - D(I_{dark})} \quad (5)$$

where I_{flat} is the image of the chamber without sample. $I_{norm,\,n}$ corresponds to the corrected transmission intensity T and will be shown as a percentage in the text.

Interpretation of the Corrected Images. Figure 3a and Figure 3b show the neutron image of the CNF-treated canvas before and after the image correction, respectively: intensity correction accounting for beam signal instability, dark, flat, and reduction of noise. Figure 3c and Figure 3d show the plot of the signal with time from an area on the canvas sample directly exposed to the chamber environment, i.e., unshielded (marked by a white square indexed ii. in Figure 3a,b). In Figure 3c, the signal measured on the raw image shown in Figure 3a corresponds to the mean of the pixel intensity of the image.

https://dx.doi.org/10.1021/acsapm.0c01073
ACS Appl. Polym. Mater. 2021, 3, 777−788

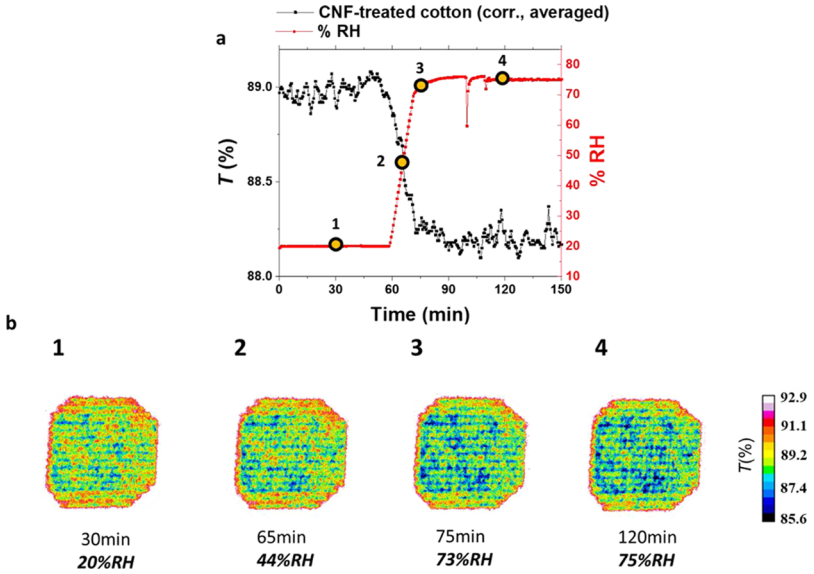

Figure 4. (a) T(%) vs time for cotton CNF-treated canvas together with four average neutron transmission images (b) (1−4) corresponding to different exposure times and RH values. Red to blue areas on the images indicate areas from high to low T(%), hence moisture content from low to high.

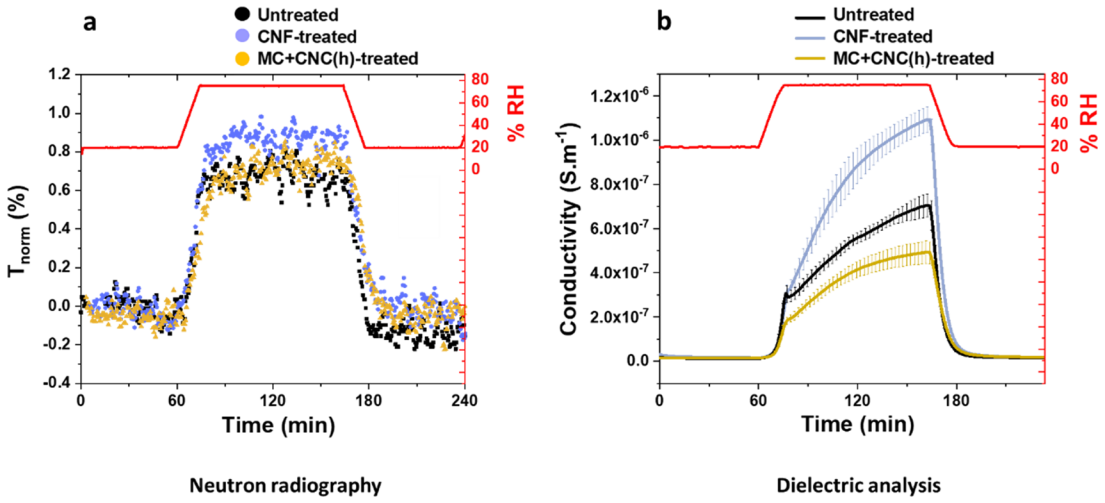

Figure 5. In (a), mean percentage in normalized T(%) measured by neutron radiography for untreated (black) and CNF-treated (blue) and MC +CNC(h)-treated (yellow) cotton for one RH cycle (red) (20−75−20%RH, 4%RH/min). These results are compared with dielectric analysis (DEA) results (averaged data with error bars) (b), which show the increase in conductivity with an increase in RH for the canvas samples subjected to one cycle RH (red).

After correction, a transmission image can be obtained, and as such, the mean percentage of transmission T(%) calculated in the unshielded area is presented in Figure 3d. An area beside the cotton sample (green rectangle indexed i. in Figure 3a,b) was also measured to check the validity of the correction and to confirm that results were not affected by variations in RH level in the chamber. The area chosen was different from the one used to measure the beam signal and that used in the correction (Figure 2a). Results gave a linear and flat transmission line demonstrating the efficiency of the correction (see Figure S1a in the Supporting Information).

In Figure 3b, the neutron radiography after correction of the cotton canvas exposed to the RH program (here at 75%RH, i.e., transmission of wet state) shows a distribution of colors that correspond to values of transmission T(%). The increased water vapor content within the sample cell and within the sample itself augments the presence of hydrogen-containing material (water vapor), leading to a decrease in neutron transmission.

Figure 4a is a development of the data shown in Figure 3d, where the signal has been further averaged (moving average using four images for each average) and shows less noise.

Four averaged neutron transmission images corresponding to different exposure times and RH levels are shown in Figure 4b. Images 1−4 represent the transmission level for the indicated times and selected RH values from 30 min (20%RH) to 120 min (75%RH). The images indicate a visible increase in blue colored areas associated with low T(%) in the neutron beam as RH increases from the starting position at 20%RH shown at 30 min to 44%RH at 65 min indicated by neutron images 1 and 2, in Figure 4b. The yellow and orange colors correspond to high values of T(%) (i.e., lower moisture content). In contrast, the green and blue regions correspond to values with lower T(%) (i.e., higher moisture content).

https://dx.doi.org/10.1021/acsapm.0c01073
ACS Appl. Polym. Mater. 2021, 3, 777−788

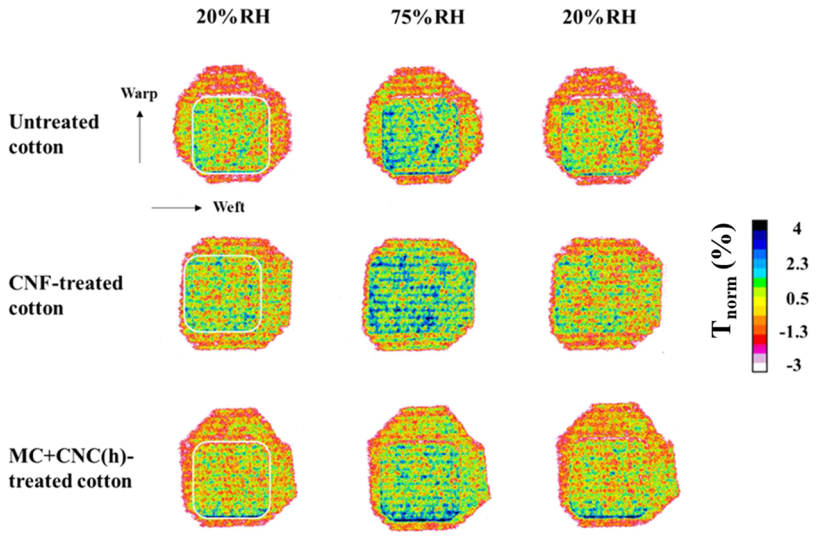

Figure 6. Neutron normalized transmission images of an untreated and a CNF-treated and MC+CNC(h)-treated degraded cotton canvases. The normalization of the transmission was performed to the "dry state" (i.e., 20%RH, end equilibration). These images show the distribution of moisture during a 20−75−20%RH cycle at end plateau values. Samples were all oriented in the same way (weft = horizontal, warp = vertical).

The results of the neutron experiment performed on the CNF-treated sample and presented in Figure 4 (both (a) and (b)) indicate that the response of the sample to the RH increase is almost immediate and that neutron radiography is sensitive enough to pick up a change in moisture content in the canvas.

Hygroscopic Response of Consolidants for Painting Canvases. Following the development of the protocol for neutron imaging measurements under cycling RH and subsequent image correction, this protocol of testing was used to investigate the impact of the CNF and MC+CNC(h) treatments on the hygroscopic response of the degraded cotton canvas. The effect of moisture sorption on neutron radiography expressed in terms of change in normalized transmission T_{norm} (%) with RH is shown for one cycle (20−75−20%RH) in Figure 5a for cotton canvases untreated and treated. The normalized transmission T_{norm} (%) was calculated by first dividing T(%) by the average value in T(%) measured at the "dry state", i.e., the end of the first 20%RH plateau (n = 5), to compensate for the different thicknesses of the samples. The quotient obtained was subsequently subtracted from 100% to facilitate comparison between neutron and dielectric measurements with RH cycles.

The CNF-treated sample shows a higher response to moisture than does the untreated and MC+CNC(h)-treated samples, as shown by the T_{norm} (%) values measured at the end of the 75%RH plateau. Normalized transmission values, reach 0.59, 0.60, and 0.73% at 75%RH (end plateau, first RH cycle) for the untreated, the MC+CNC(h)-treated and the CNF-treated canvases, respectively. The onset time at which moisture sorption occurs for the MC+CNC(h) sample is also delayed with respect to the other two samples. Untreated and CNF-treated samples respond slightly ahead of the MC +CNC(h)-treated sample. This can be seen at the start of the 75%RH plateau (Figure 5a). Finally, a difference in the times at which desorption occurs is observed. This occurs more rapidly for the untreated than the treated samples.

The dielectric data averaged for each sample type exposed to the same RH cycles are presented in Figure 5b. The results confirm the higher hygroscopic behavior of the CNF-treated sample. The relationship in eq 2 was found applicable for the four frequencies used, thus confirming that the loss permittivity ε'' measurement was due to an ionic conduction mechanism.[31] In Figure 5b, the CNF-treated sample attains a higher value of conductivity both at the start and end of the 75%RH plateau in comparison with the MC+CNC(h)-treated and the untreated samples. At low RH (i.e., 20%RH), the value for conductivity is low ($1.2-1.6 \pm 0.1 \times 10^{-8}$ S/m). In the dry state, this is expected as it is well known that cellulose behaves as an insulator. With the increase in RH to 75%RH, there is a marked change in conductivity, which increases to $7.0 \pm 0.5 \times 10^{-7}$ S/m, for the untreated sample and up to two orders of magnitude to $10.9 \pm 0.6 \times 10^{-7}$ S/m for the CNF-treated sample as measured at the end of the 75% plateau. In the case of the MC+CNC(h)-treated sample, the conductivity only reaches $4.9 \pm 0.5 \times 10^{-7}$ S/m. This can be clearly seen in Figure 5b.

The higher conductivity measured at 75%RH for the CNF-treated sample seen for the RH cycle is associated with the known behavior of cellulose. Recent studies on cellulose nanocrystals (CNC) have demonstrated that this other type of nanocellulose compound alone also has a strong affinity for water.[39]

The cellulose ether and CNC used to make the heptane-based nanocomposite consolidant have been chemically derivatized through silylation to be dissolved and dispersed in apolar solvents.[33] This derivatization followed a process in which the hydrogen of all hydroxide groups was replaced by trimethylsilyl groups. In the absence of hydrophilic hydroxide groups, the water sorption of these compounds is significantly reduced. Also, a recent study by Orasugh et al.[40] has demonstrated that the addition of CNC added at low concentrations to the cellulose ether methylcellulose (MC) forms a nanocomposite with improved mechanical and moisture barrier (i.e., lower water sorption) properties. This results in the formation of a hydrogen-bond cross-linked structure such that the hydrogens present on the CNC or MC backbone are no longer available for bonding with water.

https://dx.doi.org/10.1021/acsapm.0c01073
ACS Appl. Polym. Mater. 2021, 3, 777−788

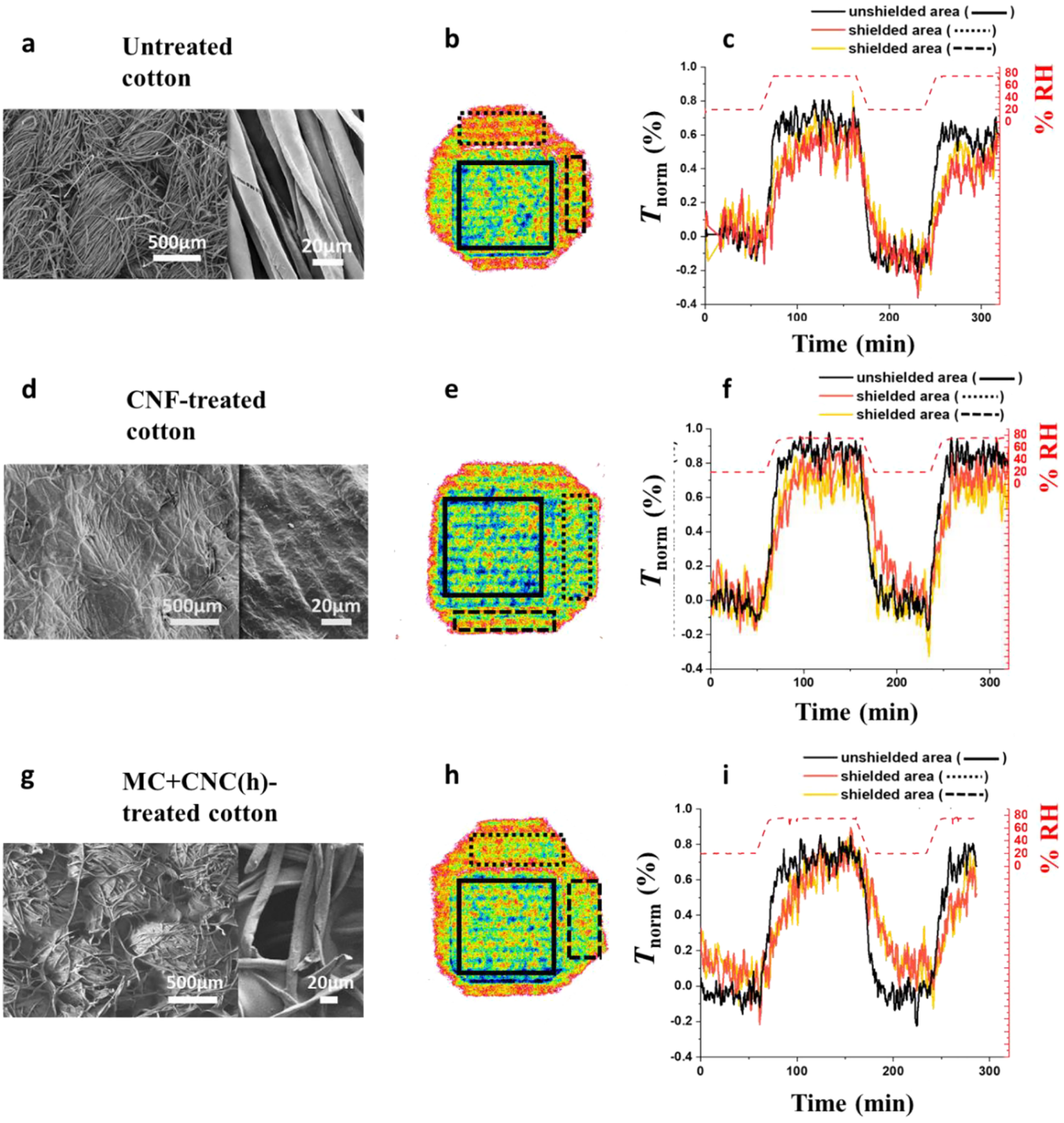

Figure 7. FEG-SEM images, T_{norm} (%) maps, and profile of the untreated (a–c), CNF-treated (d–f), and MC+CNC(h)-treated (g–i) cotton canvas. Maps of T_{norm} (%) already shown in Figure 6 at 75%RH (1st cycle, end plateau) of untreated (b) and CNF-treated (e) cotton canvas samples show the area exposed to RH (black full line, 7.4 × 7.4 mm^2) as well as the two areas, shielded to RH (both black dotted line), used to calculate the variations in T_{norm} (%) under RH cycling (20–75%RH, 4%RH/min).

Therefore, the results of the dielectric measurements confirm the lower hydrophilic behavior expected for the MC+CNC(h)-treated sample in comparison with the untreated and CNF-treated canvases.

The behavior of the three samples during the 75%RH plateau of the RH cycle (Figure 5b) also shows a difference. The conductivity of the untreated sample increases linearly at 75%RH, without attaining equilibrium. In contrast, the treated samples exhibit a two-stage process, as shown by the change in the slope after approximately 30 min into the 75%RH plateau. It seems that the presence of CNF improves the diffusion of water into the sample, and transmission approaches equilibrium at a faster rate than the untreated sample. In the case of the hydrophobic MC+CNC(h) sample, the sorption of water is less, and equilibrium is approached faster than either of the other two samples.

Mapping Moisture. Figure 6 shows the normalized transmission images of untreated and CNF-treated and MC

https://dx.doi.org/10.1021/acsapm.0c01073
ACS Appl. Polym. Mater. 2021, 3, 777–788

Table 1. T_{norm} (%) Measured on the Shielded and Not Shielded Areas of the Untreated, CNF-Treated Cotton, and MC +CNC(h)-Treated Canvases as Defined in Figure 7[a]

Samples	75%RH plateau (1st RH cycle) Area	$T_{norm,start}$ (%) Normalized transmittance Start point (t=74min) [%]	$T_{norm,end}$ (%) Normalized transmittance End point (t=164min) [%]	$T_{norm,end}$ (%) - $T_{norm,start}$ (%) [%]
Untreated cotton	Shielded ( )	0.15	0.54	*+0.39*
	Shielded (---)	0.35	0.60	*+0.25*
	Not shielded ( )	0.60	0.68	*+0.08*
CNF-treated cotton	Shielded ( )	0.50	0.78	*+0.28*
	Shielded (---)	0.59	0.63	*+0.04*
	Not shielded ( )	0.79	0.85	*+0.06*
MC+CNC(h)-treated cotton	Shielded ( )	0.25	0.71	*+0.46*
	Shielded (---)	0.24	0.72	*+0.48*
	Not shielded ( )	0.52	0.72	*+0.20*

[a]The results are given for the beginning and end of the first 75%RH plateau. The values in T_{norm} (%) at the start and endpoint of the 75%RH plateau correspond to average values (n = 5).

+CNC(h)-treated cotton canvases after corrections and after 60 min equilibration at 20%RH and 90 min at 75%RH. The highest level of normalized transmission T_{norm} (%) hence higher moisture content, as indicated by dark blue color, is mainly localized in the area of the sample exposed to the chamber cell environment (i.e., center square opening with round edges seen on the sample).

From the images, it can be seen that, for all the samples, there is also a distinct overall increase in T_{norm} (%), particularly important in the unshielded areas of the sample (white square in Figure 6), indicated by the increase in green/blue areas at RH 75%, which is then lost at 20%RH. On dehumidification, at the rate of 4%RH /min, there is a loss of blue regions indicating loss of moisture. However, in the cases of the CNF-treated and MC+CNC(h)-treated samples, there is some residual effect as also seen in Figure 5a where T_{norm} (%) values do not return to original values.

The images in Figure 6 agree with the data shown in Figure 5a, where the CNF-treated sample shows higher T_{norm} (%) values than the untreated sample. The evaluation of moisture content of the samples during RH cycle would require prior calibration using samples with a known amount of absorbed water[24] or absorption of different water layer thickness.[41]

Role of the Frame in Restricting Moisture Uptake. Additionally, the frame is shown to offer protection against moisture diffusion to areas beneath it that are not directly exposed to the chamber environment. This is particularly noticeable in Figure 6 for the untreated sample at 75%RH. The differences in T_{norm} (%) between shielded (sample underneath metal frame) and unshielded areas were further investigated. Figure 7c,f,i shows changes in T_{norm} (%) with time measured for areas shown in Figure 7b,e,h unshielded to RH (solid line on neutron image) and those shielded to the RH program (dashed and dotted lines on neutron images). The results are expressed in terms of T_{norm} (%) and RH against time from different areas of the sample and demonstrate the protective action of the frame. For all the samples, there is some delay with the change in RH in shielded areas, i.e., under the frame (red, orange), compared to the unshielded area (black). Moisture sorption and desorption in areas not shielded to the RH-controlled environment are almost immediate and follow the variations in RH (red dashed line). On the contrary, the two shielded areas, which behave similarly, show a delay in response characterized by a slow increase in T_{norm} (%) during the first 45 min at 75%RH for both the first and second RH cycles. This trend is particularly pronounced for the untreated and MC+CNC(h)-treated canvases.

During the first 20−75%RH transition, T_{norm} (%) measured from the two areas of the untreated canvas shielded from RH (top dotted and right side dashed black rectangles in Figure 7b and orange, red lines in Figure 7c) increases by 0.15 and 0.35% (see Table 1), respectively, whereas T_{norm} (%) measured for the area not shielded from RH (in Figure 7, black square (b) and black line (c)) reaches a value of 0.60% in the same time. During the 75%RH plateau (from start to end), T_{norm} (%) of the unshielded area increases by an additional 0.08% only, whereas, for the shielded ones, T_{norm} (%) gradually increases to reach 0.54% (+0.39%) and 0.60% (+0.25%) respectively, after 90 min (see Table 1).

The MC+CNC(h) treatment, similarly, slows down the diffusion of moisture to the shielded areas with T_{norm} (%) around 0.25 and 0.24% (Table 1), which is in contrast with the 0.52% measured in the unshielded area at the beginning of the first equilibration at 75%RH. In addition, Figure 7i also shows that the MC+CNC(h) treatment compared to the untreated and CNF-treated samples greatly slows down moisture desorption from the shielded areas of the canvas. These results are of importance as they indicate that the MC +CNC(h) treatment could increase the buffer effect of the canvas to water vapor.

https://dx.doi.org/10.1021/acsapm.0c01073
ACS Appl. Polym. Mater. 2021, 3, 777−788

For the CNF-treated sample, the reduction in moisture sorption for the areas under the frame compared to the exposed area is far less pronounced. As reported in Table 1, in the shielded areas delimited by dotted and dashed lines (black rectangles) in Figure 7e, T_{norm} (%) reaches already 0.50 and 0.59%, respectively, while the unshielded area (black square Figure 7e) is at 0.79% just after the first RH transition from 20 to 75%RH. This significant difference between untreated and CNF-treated canvas indicates that moisture diffusion across the canvas is facilitated by the CNF treatment.

Indeed, in Figure 7a and Figure 7d , the FEG-SEM images of the surface of the cotton canvas before and after treatment, respectively, reveal that the CNF treatment forms a layer (around 10 μm for the side with 15 g/m^2 surface coverage) as already reported elsewhere.[17] The film deposited on top of the canvas is not only hygroscopic, as shown by neutron and high conductivity measured by dielectric measurements (Figure 5b), it also effectively reduces the path for moisture diffusion. Therefore, it increases the rate of moisture transfer across the canvas to areas not immediately exposed to moisture. This finding could also explain the higher initial rate of increase in conductivity and two steps response observed previously by dielectric analysis for the treated samples (Figure 5b). In the case of the MC+CNC-treated sample, there is no layer formation, and the treatment penetrates more into the sample as shown in Figure 7g in comparison to the layer seen in the CNF-treated sample Figure 7d.

CONCLUSIONS

The sample cell specially designed for our application has been successfully used to test the programmed rate of moisture sorption and desorption in small canvas samples by neutron radiography. Its small size as well as the reproducible sample positioning and exposure to linear programmed RH changes at controlled temperature enabled us to correlate changes observed in neutron images with data measured under the same conditions by dielectric analysis. It also demonstrates the potential of neutron radiography to follow real-time moisture diffusion dynamics. The rapid response measured for the samples to RH increase and decrease could be readily correlated to change in moisture content. A differential response was recorded for the CNF- and MC+CNC(h)-treated degraded cotton canvases exposed to the same RH program. The increase in T_{norm} (%) values is greater for the CNF-treated canvas than for the MC+CNC(h) canvas. The difference between the two treatments using hydrophilic and hydrophobic materials as well as between untreated and treated canvases, which was confirmed by complementary dielectric measurements, is of importance for conservators in planning their selection of materials for treatment. The fact that the MC+CNC(h) treatment, for example, tends to slow down moisture diffusion during RH transitions and RH plateaux is also of value as it demonstrates the protective action of this treatment with respect to their behavior toward fluctuations in RH. Additional evidence that changes did occur with RH was seen in that the frame holding the sample offered some protective action, and unexposed areas showed a slower response to moisture. This phenomenon was more pronounced for the untreated and MC+CNC(h)-treated canvas. The hygroscopic CNF coating, in comparison, increases moisture diffusion across the canvas, hence increases the responsiveness of the entire painting to moisture (unexposed and exposed areas) but simultaneously offers a more homogeneous distribution of this moisture. This is particularly interesting to know that a close relationship exists between the moisture content and mechanical properties for these canvas samples. Moisture gradients, hence gradients in mechanical properties, within paintings on canvas can lead to building up of tension, causing eventual damage to the paint layer. Additional assessments are required to establish whether the higher moisture diffusion measured for the treated canvas is beneficial to a painting in reducing the risks of mechanical failures. With that perspective, neutron radiography could further be used to follow the transversal moisture diffusion processes occurring within treated canvases. It would be particularly interesting to observe the difference in behavior between the MC+CNC(h) nanocomposite and CNF-treated canvases since, in the latter case, the treatment creates a superficial coating.

ASSOCIATED CONTENT

Supporting Information

The Supporting Information is available free of charge at https://pubs.acs.org/doi/10.1021/acsapm.0c01073.

Comparison of the signal measured after image correction in an area besides the canvas sample and on the sample (PDF)

AUTHOR INFORMATION

Corresponding Author

Alexandra Bridarolli − *Eastman Dental Institute, London WC1E 6DE, U.K.; Getty Conservation Institute, Los Angeles, California 90049, United States;* orcid.org/0000-0002-0114-751X; Email: abridarolli@getty.edu

Authors

Marianne Odlyha − *Department of Biological Sciences, Birkbeck, University of London, London WC1E 7HX, U.K.*

Genoveva Burca − *ISIS Facility, Rutherford Appleton Laboratory, Oxon OX11 0QX, U.K.*

John C. Duncan − *Lacerta Technology Ltd., Shepshed LE12 9GX, U.K.*

Freddie A. Akeroyd − *ISIS Facility, Rutherford Appleton Laboratory, Oxon OX11 0QX, U.K.*

Andie Church − *ISIS Facility, Rutherford Appleton Laboratory, Oxon OX11 0QX, U.K.*

Laurent Bozec − *Eastman Dental Institute, London WC1E 6DE, U.K.; Faculty of Dentistry, University of Toronto, Toronto, ON M5G 1G6, Canada*

Complete contact information is available at: https://pubs.acs.org/10.1021/acsapm.0c01073

Notes

The authors declare no competing financial interest.

ACKNOWLEDGMENTS

The authors are particularly thankful to Robert Fischer and Dominique Derome from EMPA (Dübendorf, Switzerland) and Dr. David Mannes from the Paul Scherrer Institute (Villigen, Switzerland) for their suggestions and help throughout the development of this study. They would also like to thank Chloe Pearce for helping with the samples preparation at ISIS and Dr. James Taylor and Sarah Langhman for granting access to ISIS Chemistry and Sample preparation laboratory. Finally, the authors are also grateful to Dr. Romain

Bordes and Dr. Oleksandr Nechyporchuk from Chalmers University (Gothenburg, Sweden) and Dr. Manfred Anders from the Zentrum für Bucherhaltung (Leipzig, Germany) for providing us with the nanocellulose-based treatments and their support. This study was supported by a co-funding from the H2020 Nanorestart European Project and the Engineering and Physical Sciences Research Council (EPSRC) through the Centre for Doctoral Training In Science and Engineering in Arts, Heritage, and Archaeology (SEAHA).The neutron data were acquired at the STFC ISIS Neutron and Muon Source from the experiment RB1820595 (DOI: 10.5286/ISIS.E.RB1820595).

REFERENCES

(1) Oriola, M.; et al. Looking beneath Dalí's paint: Non-destructive canvas analysis. *Anal. Methods* **2014**, *6*, 86−96.
(2) Hackney, S. Paintings on Canvas: Lining and Alternatives. *Tate Paper* 2004.
(3) Hedley, G.; Odlyha, M.; Burnstock, A.; Tillinghast, J.; Husband, C. A study of the mechanical and surface properties of oil paint films treated with organic solvents and water. *J. Therm. Anal.* **1991**, *37*, 2067−2088.
(4) Macbeth, R.; Odlyha, M.; Burnstock, A.; Villers, C.; Bruce-Gardner, R. Evaluation of moisture treatment of fabric-supported paintings. in *ICOM Committee for Conservation 10th triennial meeting;* Washington, DC, 22−27 August 1993. : preprints (1993)
(5) Ackroyd, P.; Phenix, A.; Villers, C. Not lining in the twenty-first century: Attitudes to the structural conservation of canvas paintings. *Conserv.* **2002**, *26*, 14−23.
(6) Hackney, S.; Reifsnyder, J.; te Marverde, M.; Scharff, M. Lining easel paintings. in *The conservation of easel paintings* ed. Stoner, J. H.; Rushfield, R. Routledge, 2012.
(7) Feller, R. L.; Curran, M.; Bailie, C. Photochemical Studies of Methacrylate Coatings for the Conservation of Museum Objects. in *Photodegradation and Photostabilization of Coatings* 183−196 1981, DOI: 10.1021/bk-1981-0151.ch013.
(8) McGlinchey, C. et al. Lining and Consolidating Adhesives: Some New Developments and Areas of Future Research. in *Adhesives and Consolidants for Conservation: Research and Applications,* Canadian Conservation Institute: (2011).
(9) Azeredo, H. M. C. d. Nanocomposites for food packaging applications. *Food Res. Int.* 2009 *42*, 1240−1253, DOI: 10.1016/j.foodres.2009.03.019, .
(10) Kaboorani, A.; Auclair, N.; Riedl, B.; Landry, V. Physical and morphological properties of UV-cured cellulose nanocrystal (CNC) based nanocomposite coatings for wood furniture. *Prog. Org. Coatings* **2016**, *93*, 17−22.
(11) Nechyporchuk, O.; et al. On the potential of using nanocellulose for consolidation of painting canvases. *Carbohydr. Polym.* **2018**, *194*, 161−169.
(12) Bridarolli, A.; Nualart-Torroja, A.; Chevalier, A.; Odlyha, M.; Bozec, L. Systematic mechanical assessment of consolidants for canvas reinforcement under controlled environment. *Herit. Sci.* **2020**, *8*, 1−12.
(13) Lavoine, N.; Bras, J.; Desloges, I. Mechanical and barrier properties of cardboard and 3D packaging coated with micro-fibrillated cellulose. *J. Appl. Polym. Sci.* **2014**, *131*, 40106.
(14) Lee, K. Y.; Aitomäki, Y.; Berglund, L. A.; Oksman, K.; Bismarck, A. On the use of nanocellulose as reinforcement in polymer matrix composites. *Compos. Sci. Technol.* **2014**, *105*, 15−27.
(15) Osong, S.; Norgren, S.; Engstrand, P. Processing of wood-based microfibrillated cellulose and nanofibrillated cellulose, and applications relating to papermaking: a review. *Cellulose* **2016**, *23*, 93−123.
(16) Lin, N.; Dufresne, A. Nanocellulose in biomedicine: Current status and future prospect. *Eur. Polym. J.* **2014**, *59*, 302−325.
(17) Bridarolli, A.; et al. Evaluation of the adhesion and performance of natural consolidants for cotton canvas conservation. *ACS Appl. Mater. Interfaces* **2018**, *10*, 33652−33661.
(18) Bridarolli, A. *Multiscale approach in the assessment of nanocellulose-based materials as consolidants for painting canvases.* University College London (UCL): 2019.
(19) Hedley, G. Relative humidity and the stress/strain response of canvas paintings: Uniaxial measurements of naturally aged samples. *Stud. Conserv.* **1988**, *33*, 133−148.
(20) Mecklenburg, M. F. *Some aspects of the mechanical behavior of fabric supported paintings.* (1982).
(21) Burca, G.; et al. Exploring the potential of neutron imaging for life sciences on IMAT. *J. Microsc.* **2018**, *272*, 242−247.
(22) Mawodza, T.; Burca, G.; Casson, S.; Menon, M. Wheat root system architecture and soil moisture distribution in an aggregated soil using neutron computed tomography. *Geoderma* **2020**, *359*, 113988.
(23) Mannes, D.; et al. Water vapour diffusion through historically relevant glutin-based wood adhesives with sorption measurements and neutron radiography. *Wood Sci. Technol.* **2014**, *48*, 591−609.
(24) Boon, J. J.; et al. Neutron radiography for the study of water uptake in painting canvases and preparation layers. *Appl. Phys. A: Mater. Sci. Process.* **2015**, *121*, 837−847.
(25) Mannes, D.; Sonderegger, W.; Hering, S.; Lehmann, E.; Niemz, P. Non-destructive determination and quantification of diffusion processes in wood by means of neutron imaging. *Holzforschung* **2009**, *63*, 589−596.
(26) Hendrickx, R.; Desmarais, G.; Weder, M.; Ferreira, E. S. B.; Derome, D. Moisture uptake and permeability of canvas paintings and their components. *J. Cult. Herit.* **2016**, *19*, 445−453.
(27) Hendrickx, R.; Ferreira, E. S. B.; Boon, J. J.; Desmarais, G.; Derome, D.; Angelova, L.; Mannes, D.; Kaestner, A.; Huinink, H.; Kuijpers, K.; Voogt, B.; Richardson, E. Distribution of moisture in reconstructed oil paintings on canvas during absorption and drying: A neutron radiography and NMR study. *Stud. Conserv.* **2017**, *62*, 393−409.
(28) Mannes, D.; Schmid, F.; Wehmann, T.; Lehmann, E. Design and Applications of a Climatic Chamber for in-situ Neutron Imaging Experiments. *Phys. Procedia* **2017**, *88*, 200−207.
(29) Urquhart, A. R. 15−The mechanism of the adsorption of water by cotton. *J. Text. Inst. Trans.* **1929**, *20*, T125−T132.
(30) Hill, C. A. S.; Norton, A.; Newman, G. The water vapor sorption behavior of natural fibers. *J. Appl. Polym. Sci.* **2009**, *112*, 1524−1537.
(31) Le Bras, D.; Strømme, M.; Mihranyan, A. Characterization of dielectric properties of nanocellulose from wood and algae for electrical insulator applications. *J. Phys. Chem. B* **2015**, *119*, 5911−5917.
(32) Nechyporchuk, O.; et al. Accelerated ageing of cotton canvas as a model for further consolidation practices. *J. Cult. Herit.* **2017**, *28*, 183−187.
(33) Böhme, N.; et al. New treatments for canvas consolidation and conservation. *Herit. Sci.* **2020**, DOI: 10.1186/s40494-020-0362-y.
(34) Burca, G.; Kockelmann, W.; James, J. A.; Fitzpatrick, M. E. Modelling of an imaging beamline at the ISIS pulsed neutron source. *J. Instrum.* **2013**, DOI: 10.1088/1748-0221/8/10/P10001.
(35) Kockelmann, W.; et al. Status of the Neutron Imaging and Diffraction Instrument IMAT. *Phys. Procedia* **2015**, *69*, 71−78.
(36) Finocchiaro, V.; et al. The autofocusing system of the IMAT neutron camera. *Rev. Sci. Instrum.* **2013**, *84*, 093701.
(37) Akeroyd, F. A.; et al. IBEX - An EPICS based control system for the ISIS pulsed neutron and muon source. *J. Phys. Conf. Ser.* **2018**, *1021*, 012019.
(38) *Neutron radiography, data analysis (Paul Scherrer Institut PSI).* https://www.psi.ch/en/sinq/neutra/data-analysis.
(39) Natarajan, B.; et al. Dielectric Characterization of Confined Water in Chiral Cellulose Nanocrystal Films. *ACS Appl. Mater. Interfaces* **2017**, *9*, 14222−14231.
(40) Orasugh, J. T.; et al. Synthesis of methylcellulose/cellulose nano-crystals nanocomposites: Material properties and study of sustained release of ketorolac tromethamine. *Carbohydr. Polym.* **2018**, *188*, 168−180.

https://dx.doi.org/10.1021/acsapm.0c01073
ACS Appl. Polym. Mater. 2021, 3, 777−788

(41) Kang, M.; Bilheux, H. Z.; Voisin, S.; Cheng, C. L.; Perfect, E.; Horita, J.; Warren, J. M. Water calibration measurements for neutron radiography: Application to water content quantification in porous media. *Nucl. Instruments Methods Phys. Res. Sect. A Accel. Spectrometers, Detect. Assoc. Equip.* **2013**, *708*, 24−31.

https://dx.doi.org/10.1021/acsapm.0c01073
ACS Appl. Polym. Mater. 2021, 3, 777−788